JOURNAL OF GEOPHYSICAL RESEARCH, VOL. 102, NO. A7, PAGES 14,363–14,380, JULY 1, 1997

Properties of the magnetospheric hot plasma distribution deduced from whistler mode wave injection at 2400 Hz: Ground-based detection of azimuthal structure in magnetospheric hot plasmas

Vikas S. Sonwalkar,[1] D. L. Carpenter,[2] R. A. Helliwell, [2] M. Walt, [2]
U. S. Inan,[2] D. L. Caudle,[3] and M. Ikeda [4]

Abstract. Siple station VLF wave injection experiments aimed at finding the properties of the magnetospheric hot plasma were conducted for a 9-hour period between 1705 and 0210 UT on January 23-24, 1988. A special frequency versus time format, lasting 1 min and transmitted every 5 min, consisted of a sequence of pulses, frequency ramps, and parabolas, all in a 1-kHz range centered on 2400 Hz. The transmitted signals, after propagating along a geomagnetic field-aligned duct, were recorded at Lake Mistissini, Canada. At various times during the 9-hour interval the Siple signals showed features characteristic of wave-particle interactions, including wave growth, sidebands, and triggered emissions. Our observations, primarily at 2400 Hz, show that (1) there were no correlations between the initial levels, the growth rates, and the saturation levels of constant-frequency pulses; (2) in general, the values of growth rate and saturation level of two pulses injected within 30 s were nearly the same; (3) the initial level, growth rate, and saturation level showed temporal variations over 5–15 min and 1–2 hour timescales; (4) the leading edges of constant-frequency signals underwent spatial amplification; and (5) under conditions of saturation the received signal bandwidth ($\sim$ 20 Hz) remained constant over a 1-hour period, although the saturation level and growth rate varied during the same period. On the assumption that gyroresonant interactions were responsible for the observed wave growth and saturation, the timescales over which those phenomena varied provide constraints on the possible energetic electron population within the duct. In the reference frame of the duct ($L \sim 5.1$, $N_e \sim 280$ cm^{-3}) the particle fluxes showed no variation over a 30–s timescale but varied over 5–15 min and 1–2 hour timescales. The 5–15 min timescale variations indicate longitudinal structures ranging from $\sim 0.2°$ or $\sim$100 km (in the equatorial plane) for electrons with energy $E = 0.6$ keV and pitch angle $\alpha = 40°$, to $\sim 5°$ or $\sim$2800 km for electrons with energy $E = 11$ keV and pitch angle $\alpha = 80°$. The hour-long time variations indicate longitudinal structures ranging from $\sim 2°$ or $\sim$1100 km (in the equatorial plane) for electrons with energy $E = 0.6$ keV and pitch angle $\alpha = 40°$, to $\sim 45°$ or $\sim$25,000 km for electrons with energy $E = 11$ keV and pitch angle $\alpha = 80°$. We conclude that ground-based active and passive wave experiments have substantial potential for investigating properties of the hot plasma of the magnetosphere.

[1]Institute of Northern Engineering, University of Alaska Fairbanks.

[2]STAR Laboratory, Stanford University, Stanford, California.

[3]Naval Postgraduate School, Monterey, California.

[4]Musashi University, Tokyo 176, Japan.

Paper number 96JA03047.
0148-0227/97/96JA-03047$09.00

1. Introduction

Active whistler mode radio probing of the hot plasma of the Earth's magnetosphere has been conducted at various times between 1973 and 1988 at Siple Station, Antarctica, and at receiving sites in the northern hemisphere conjugate region [*Helliwell and Katsufrakis*, 1974; *Helliwell*, 1988]. Until the mid 1980s most of the experiments with the Siple VLF transmitter were devoted to describing various properties of the received signals and interpreting them in terms of

path locations, propagation parameters, and magnetospheric wave-particle interaction mechanisms [see *Helliwell*, 1988; *Sonwalkar*, 1995, and references therein]. Given the substantial progress that was made in these areas, it became possible to seek a further objective, the use of ground-observed whistler mode signals as probes of spatial structure and other properties of the hot plasmas of the magnetosphere. The purpose of this and a companion paper by *Carpenter et al.* [this issue] (hereinafter referred to as paper 2) is to identify and discuss the hot plasma probing potential of a special sequence of Siple signals transmitted during a 9-hour period in the austral summer of 1987-1988.

A model of a ground-to-ground whistler mode wave injection experiment is sketched in Figure 1a. Signals radiated from a transmitting antenna T illuminate the bottomside of the ionosphere over an extended region, and some fraction of the energy is injected into the magnetosphere. Much of this energy (not illustrated) propagates in an unducted mode and does not reach conjugate ground stations. Instead, the ray direction tends to depart substantially from the direction of the geomagnetic field and the ray path may follow a trajectory back and forth across the equator between magnetospheric reflection points that are located well above the $F2$ layer of the ionosphere [*Kimura*, 1966; *Smith and Angerami*, 1968; *Edgar*, 1976; *Sonwalkar*, 1995]. As illustrated, some fraction of the upgoing energy can become trapped within geomagnetic field-aligned ducts, discrete paths along which the signals can be guided to the conjugate hemisphere [e.g., *Helliwell*, 1965]. Upon exiting the highly refracting ionosphere, the ducted signals spread in the Earth-ionosphere waveguide and may be received at a ground station R.

The multipath nature of the propagation tends to complicate the experiment in that the signals at a given frequency received from two or more ducts may overlap one another in time. However, overlap can often be avoided if the frequency of the transmitter varies sufficiently rapidly in time, as for example in the case of

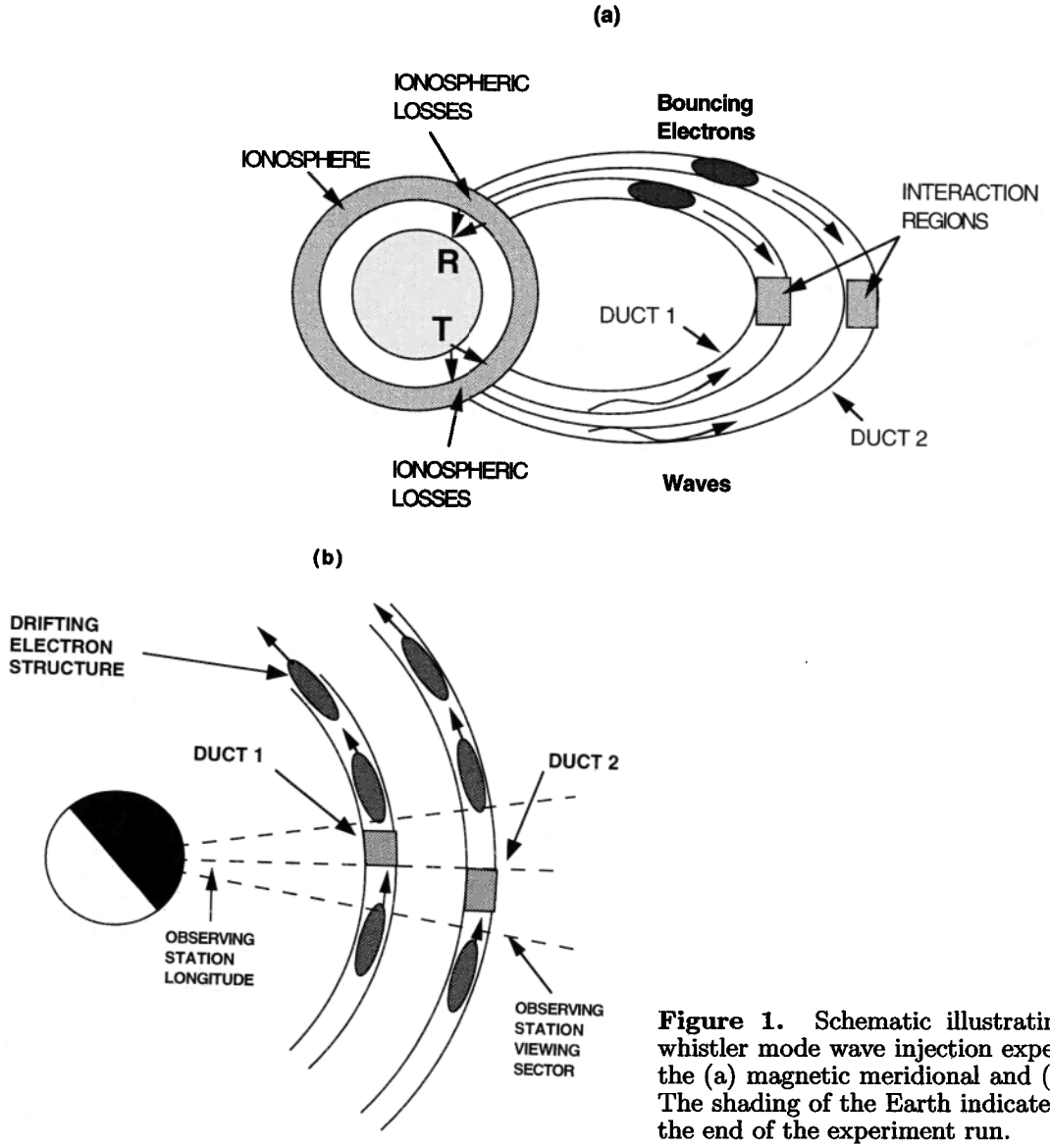

Figure 1. Schematic illustrating ground-to-ground whistler mode wave injection experiments projected in the (a) magnetic meridional and (b) equatorial planes. The shading of the Earth indicates the local time near the end of the experiment run.

frequency ramps, or if the group delays along the ducts differ by amounts comparable to the duration of individual elements in the transmission format.

The intensity of the transmitter signal at the ground receiver, which in general is the net signal from the output of various ducts, depends on (1) the coupling of the transmitter signal to the ducts (ionospheric transmission coefficients, D and E region absorption, duct size, signal coupling to the duct, etc.); (2) wave-particle interactions in the magnetosphere; and (3) coupling from the exit points of the ducts to the receiver.

In this study the observed frequency versus time, or dispersion, properties of the received signals are first used to determine the radial locations within the geomagnetic field of the discrete signal paths and the background cold plasma densities along those paths. The L value for a path is estimated from information on relative variations in group delay with frequency, while the electron density along the path at the equator is obtained from the observed group delay at a particular frequency [e.g., *Carpenter and Smith*, 1964].

The next step is to seek evidence about the propagation factors summarized in points 1 and 3. Once such evidence is obtained and some assumptions are made about the size of the active propagation ducts, properties of the observed amplitude spectra such as exponential growth, saturation, sideband generation, and triggering of emissions may be interpreted in terms of the distribution in phase space of hot magnetospheric electrons and their variations with time at the L shell of propagation. Figure 1b shows the concept. Indicated are the equatorial cross sections of two ducts; it is assumed that the ducts corotate with the Earth. Because of differential motion of the cold plasma of the duct and the hot electrons that are in approximate resonance with the ducted waves, the structure in the hot electrons will be registered as temporal changes in the wave activity. Below we develop this concept in terms of a multihour case study of Siple signal receptions. Information about the hot plasma is obtained from transmissions at a single frequency, 2400 Hz. Paper 2 discusses information derived from variations in signal receptions with frequency and pays special attention to ways of separately identifying the effects of spatial and temporal growth.

2. Experiment Description

The facilities in the wave injection experiments have been described in previous papers [e.g., *Helliwell*, 1988, and references therein]. A schematic illustration of the experiment is given in Figure 2a, which for simplicity shows a single duct along which signals propagate from Siple Station to Lake Mistissini, Canada. Along the magnetospheric portion of the path the relatively weak injected signal may undergo temporal growth of order 30 dB within a spatially limited interaction region [*Carlson*, 1987; *Carlson et al.*, 1990, and references therein]. Figure 2b shows the crossed 42-km horizontal transmitting dipoles used, while Figure 2c shows schematically the expected differences among left hand, right hand, and linearly polarized signals in their penetration of the overhead ionosphere.

Our case study is based on broadband VLF recordings at the conjugate ground station Lake Mistissini, Canada, during a 9-hour Siple transmission program. The format, known as HR241, was transmitted for 1 min every 5 min between 1705 UT on January 23, 1988, and 0210 UT on January 24, 1988. As usual, it covered a 1000-Hz band centered on the selectable so-called f_{set}

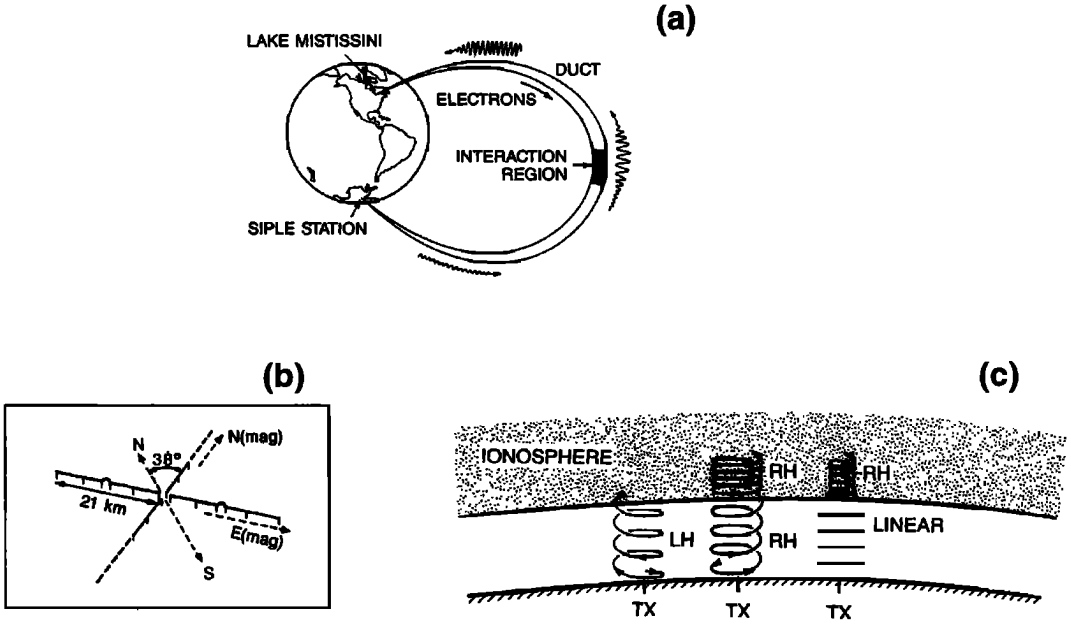

Figure 2. (a) Schematic of the Siple, Antarctica, wave injection experiment. (b) Crossed-antenna geometry. (c) Possible polarizations of the transmitter signals and their coupling to the overhead ionosphere.

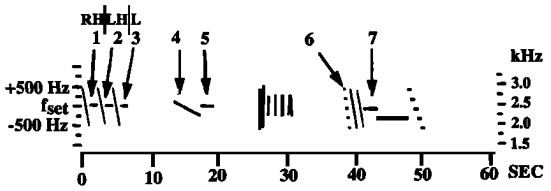

Figure 3. Diagram of the HR 241 Siple transmitter format developed for multihour studies of the magnetospheric hot plasma.

frequency, in this case 2400 Hz. The real power into the antennas varied with frequency across the 1.9–2.9 kHz transmission band and was scaled up or down in time under computer control. The maximum power from the transmitter was 72 kW (36 kW each into the two crossed elements). As noted in paper 2, the actual full power radiated at 2400 Hz was much smaller, about 427 W, due to the low antenna efficiency at VLF. The frequency-time diagram of the format is shown in Figure 3; elements numbered 1 through 7 are the ones used most in this study. Elements 1, 2, and 3 involved a series of frequency ramps and constant frequency pulses, the first ramp and pulse being transmitted with right-hand polarization, the second with left-hand polarization, and the third with linear polarization.. The three 1-s-long constant frequency pulses were ramped up to full power or 10 dB/s during the first half second. Elements 4 through 7 (and all other elements) were transmitted with right-hand polarization. Pulses 5 and 7 were both 2 s in duration, but pulse 5 was transmitted at constant (full) power, while for pulse 7 the power was ramped up to full power at 10 dB/s during the first second. The 4-s-long slow frequency ramp, number 4, was transmitted at full power as it varied linearly in frequency over a ±125-Hz range around f_{set}. Element 6 was a descending staircase of five 200-ms pulses, transmitted at full power in steps of 250 Hz beginning at f_{set} + 500 Hz.

For completeness, we note that the elements between t=26 and 31 s on the timescale were intended to investigate dispersive effects. The two frequency ramps between elements 6 and 7 were transmitted at full power and -6 dB, respectively, as a test for multipath propagation effects. The 4-s pulse at f_{set} - 250 Hz that followed element 7 consisted of two closely spaced constant frequencies, called a doublet, one at 2140 Hz and the other at 2160 Hz.

3. Observations and Data Analysis

3.1. General Features

Format HR241 was transmitted for diagnostic purposes on six different occasions during an austral summer period of approximately 5-weeks duration in December-January 1987-1988. A 9-hour period on January 23-24, 1988, was selected for detailed study because of the reception of well defined signals, mostly on a single path.

Figure 4 shows spectrograms at Lake Mistissini (LM) of the ~1 min HR241 format at six different times during the 9-hour period. Elements numbered 1, 4, 5, and 7 (see Figure 3) were identifiable on each of the six records, while other elements were detected less frequently. The variations in element definition within single 1-min periods, assuming no 1-min timescale changes in propagation conditions, are believed to be the result of element-to-element differences in the intensity, polarization, and modulation of the input signal [*Helliwell and Katsufrakis*, 1974; *Paschal and Helliwell*, 1984; *Carlson et al.*, 1985; *Helliwell et al.*, 1986a, b; *Helliwell*, 1988; *Mielke and Helliwell*, 1992; *Mielke et al.*, 1992]. Signals considered most likely to be observed are those with right-hand polarization, constant or slowly varying frequency, and duration of order 1 s or more [*Helliwell and Katsufrakis*, 1974].

Figure 5a is a spectrogram of signals 4 and 5, the slow ramp and 2-s constant power pulse, as they were received at Lake Mistissini at ~0045 UT during a period of strong signal reception that began at ~0015 UT on January 24, 1988. The chart of Figure 5b shows amplitude variations within a 100-Hz band centered on the frequency of the constant-frequency pulse and beginning just prior to the start of the pulse. The zero of the timescale of the spectrogram (Figure 5a) represents the leading edge of the 2-s constant power pulse as it was radiated at Siple station, while the zero below the amplitude record refers to t=4 s on the spectrogram scale, or the approximate time of arrival of the pulse leading edge at the receiver.

The spectrogram and the amplitude record provide complementary evidence of several hot plasma effects, including initial exponential wave growth, amplitude saturation, development of sidebands, and triggering of an emission at the termination of the transmitted pulse.

3.2. Occurrence Versus Time

Spectrographic records (such as those of Figure 4) for the entire 9-hour period were inspected and for each 1-min transmission interval the percentage of all format elements that could be visually identified was noted. Figure 6 shows the results; periods of activity with percentages of 30% or more tended to last 30 min or longer. There were eight intervals of zero activity; these were relatively brief, lasting for only two or three 5-min intervals. There were several periods when activity exceeded 50%, a 1-hour period around 2005 UT, a 15-min period near 2335 UT, and a 2-hour period around 0100 UT. The signal element observed most often in this survey was the slow ramp (element 4 in Figure 3; see also Figure 5a). The next in frequency of observation was the constant-frequency pulse that immediately followed the ramp (element 5 in Figure 3).

No whistlers were observed at Lake Mistissini during transmission periods of 1 min each 5 min or at Siple Station during recordings of 1 min each 15 min over the 9-hour period. This result is not surprising in view of the expected minimum in northern hemisphere lightning activity in January and the fact that most of the

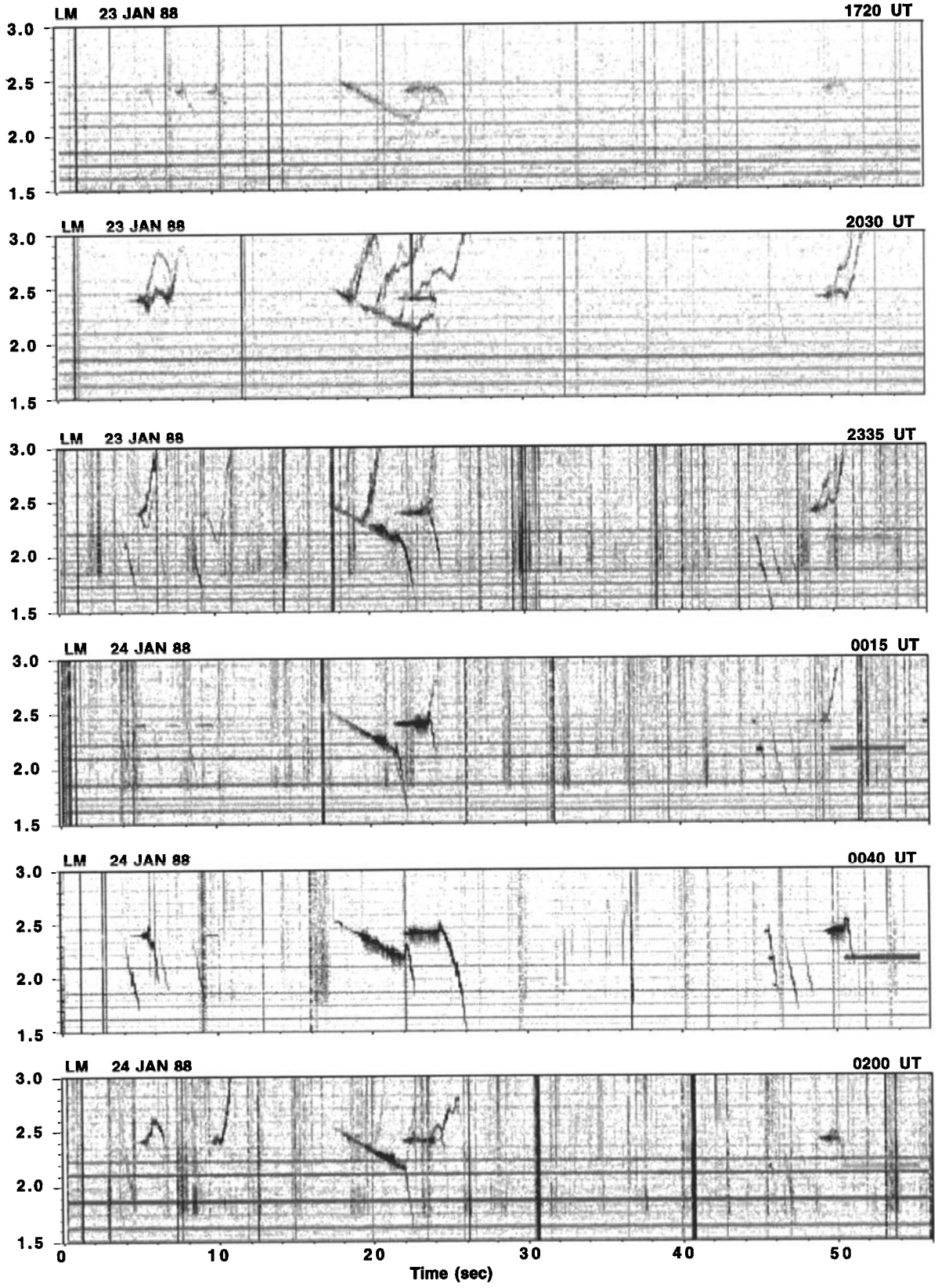

Figure 4. Spectrograms of receptions at Lake Mistissini of the ~1 min HR 241format at six different times during the 9-hour period 1700-0210 UT on January 23-24, 1988.

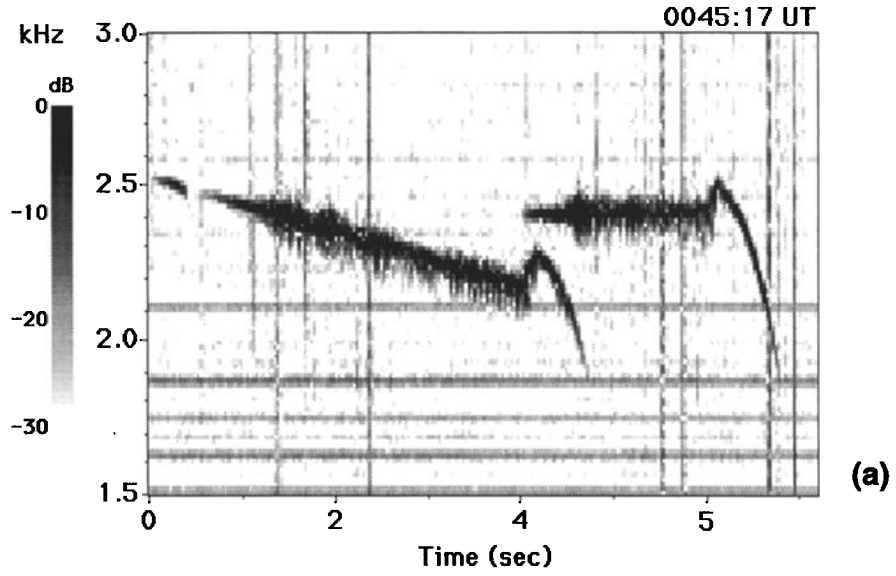

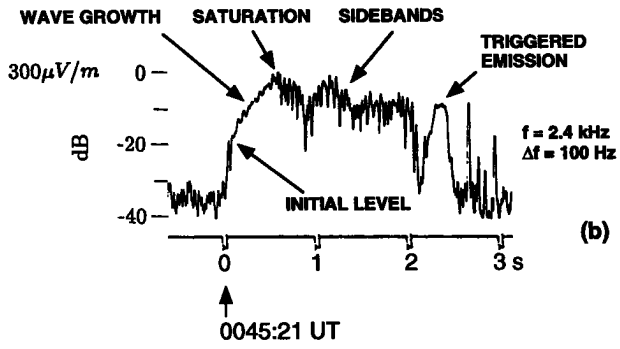

Figure 5. (a) Spectrogram of signals 4 and 5, the slow ramp, and 2-s constant power pulse, as they were received at Lake Mistissini at ~0045 UT during a period of strong activity that began at ~0000 UT on January 24, 1988. (b) Chart showing amplitude variations within a 100-Hz band centered on the frequency of the constant-frequency pulse and beginning just prior to the start of the pulse. The zero of the timescale of the spectrogram represents the leading edge of the 2-s pulse as it was radiated at Siple station, while the zero below the amplitude record refers to t=4 s on the spectrogram scale, or the approximate time of arrival of the leading edge of the 2-s pulse at the receiver.

whistlers observed near the Siple-Lake Mistissini meridian originate in the north.

3.3. Propagation of Signals: Cold Plasma Parameters

Identification of single duct and multiduct propagation was accomplished by measurements in each 1-min recording interval of the arrival time of the leading edge of the constant frequency pulse (element 5) and of its termination time and pulse length (elongation). Figure 7 shows the arrival time of element 5 with respect to its transmission time. In most cases it was possible to detect the leading edge of the signal. In a few cases in which the front edge was buried in noise, the travel time (or propagation delay) was estimated from the termination time. In general, a single duct (indicated by no measurable pulse elongation) with a duct delay T_{delay} in the range 3.9-4.1 s (measurement error ± 100 ms)

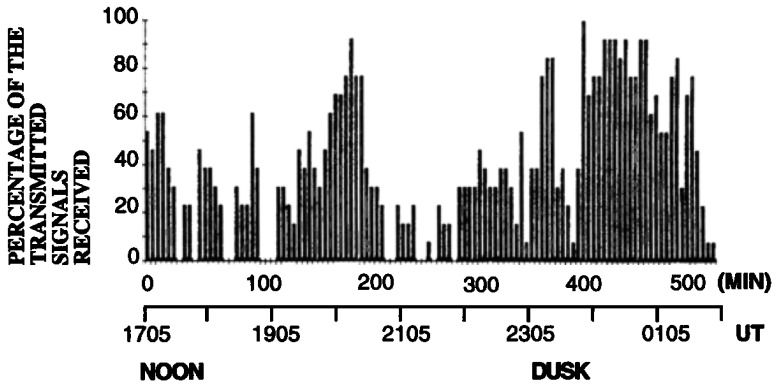

Figure 6. The percentage of all format elements that could be visually identified on 35-mm spectrographic records for each 1-min transmission interval in the 9-hour study period beginning at 1705 UT on January 23-24, 1988.

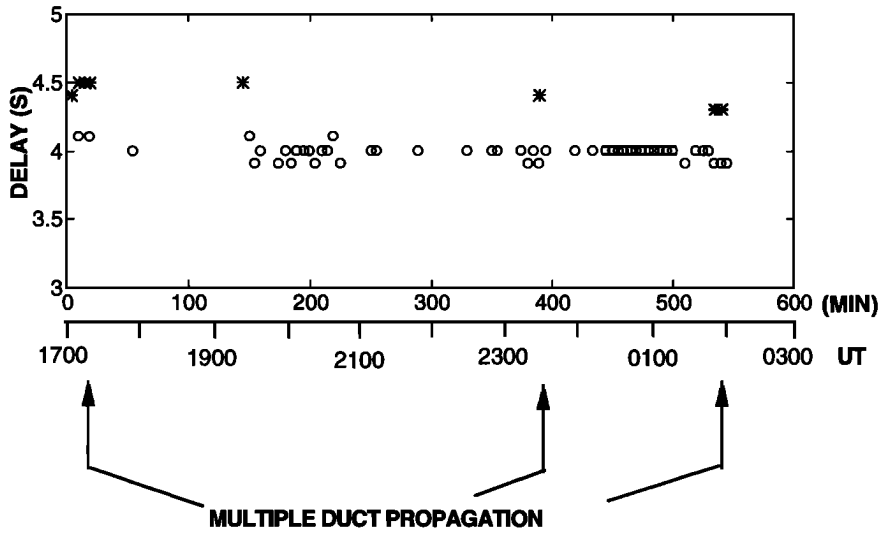

Figure 7. The measured arrival time of signal 5 with respect to its transmission time.

was active during the 9-hour period. Out of 109 transmissions, single duct propagation with $T_{\text{delay}} \sim 4$ s was detectable in 44 cases. There were clear indications of the presence of a second duct with delay 4.3-4.5 s, although signals from this duct were detected only eight times. In three of those cases, only the second duct was active, while in the other five both ducts were active. Multiduct propagation was verified in all five of these cases by the expected pulse elongations and in two of them by the arrival of two closely spaced but distinct fast ramps when a single fast ramp had been transmitted.

Dispersion analysis of the fast frequency ramps and parabolic transmissions shown in Figure 3 between t=25 and 30 s indicated that during the period of single path activity near 0100 UT the L shell of the duct was 5.1. The inferred equatorial electron density was 276 ± 10 electrons/cm^3, a dense plasmasphere value consistent with expectations for the austral summer along the Siple meridian and the quiet magnetic conditions prevailing (the maximum Kp during the preceding 12 hours was 1) [*Carpenter and Anderson*, 1992]. The observations of travel time near 4 ± 0.1 s throughout the 9-hour period suggest that the associated paths were near L=5.1 thoughout that interval.

The 200-ms jitter in the time delay measurements over the range 3.9-4.1 s can be a result of variations in the ionospheric density (order of 10%) as a function of time or indicative of fine structure within the magnetospheric duct. Since the path length along a field line is linearly proportional to the L shell of the duct, the $\pm 2.5\%$ variation in the time delays (assuming constant density) can occur as a result of injected waves propagating (and being amplified) at different times along slightly different L shells within the duct. At the L shell of 5.1 this implies structure of the order of $\Delta L \sim 0.1$, which agrees well with earlier findings of duct fine structure based on whistler and ground transmitter signal measurements [*Hamar et al.*, 1990, 1992; *Sonwalkar et al.*, 1994]. Another source of jitter in the time delays could be variations in ionospheric density due to traveling ionospheric disturbances (TIDs) [*Jursa*, 1985]. Ionospheric propagation delays (between 100 and about 1000 km) are a few hundred milliseconds [*Sonwalkar et al.*, 1984].

For a dipole model the equatorial gyrofrequency at $L = 5.1$ is 6.6 kHz, implying a half-gyrofrequency cutoff in ducted whistler mode propagation at 3.3 kHz [e.g., *Carpenter*, 1968; *Smith and Angerami*, 1968]. Thus it would be possible for signals transmitted in the 1.9-2.9 kHz range to be received at Lake Mistissini. Figure 8 shows the observed upper frequency limits of the received transmitter signals. Although the highest frequency sent was 2.9 kHz, with four exceptions the highest transmission frequency observed at the receiver was near 2.55 kHz. The estimated values of the effective radiated powers at 1.9, 2.4, and 2.9 kHz were 28, 427, and 284 W, respectively, and the ionospheric losses at 1.9 and 2.9 kHz were within 1-2 dB of each other (see paper 2 for details). Therefore, since 1.9-kHz signals were observed, 2.9-kHz signals should also have been observed, based on propagation factors alone. We suggest that the absence of signals above 2.55 kHz was due to a lack of sufficient energetic electrons to amplify the signals to detectable levels. This interpretation is consistent with recent observations of banded structures ("clouds") of electrons at within the plasmasphere ($2 < L < 6$) [*Burke et al.*, 1995]. We note, however, that emissions triggered by a few of the transmitter signals were from time to time observed up to 3.2-3.4 kHz (which corresponds to the half equatorial gyrofrequency propagation cutoff of the duct), indicating the occasional presence of energetic electron fluxes at the corresponding resonant energies.

3.4. Effects of Wave-Particle Interactions: Hot Plasma Effects

3.4.1. Nine-hour period. The initial approach to the study of temporal variations in hot plasma effects was based upon measurements of various parameters of

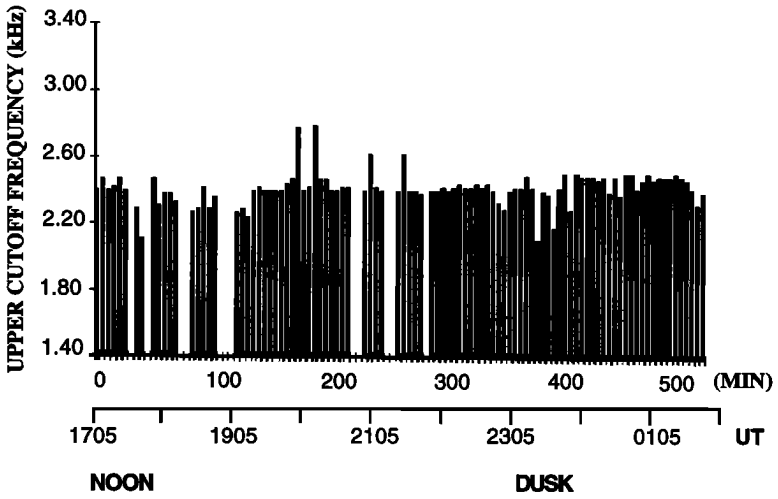

Figure 8. The observed highest frequency of Siple station transmitter signals received at Lake Mistissini during the 9-hour period.

the 2-s constant frequency pulse, element 5 in Figure 3. Amplitude records such as the one of Figure 5b were made, and within each 1-min transmission period the growth rate and saturation level were measured as well as the initial amplitude of the received pulse. Figure 9 shows the variations in the measured quantities over the 9-hour period, while Figure 10 provides scatter plots of the relationships among pairs of the quantities. (Note in Figure 9 and other similar figures to follow that signals were transmitted throughout the period indicated. In the case of amplitude measurements, a zero implies that any signal present was below the noise level of the record, which in most cases was a few decibels. In the case of growth rate a zero implies that the measurement could not be made.)

The growth rate and saturation level show several periods of activity that are consistent with the periods of higher percentage occurrence reported in Figure 6, and in general there appears to be a positive correlation between percentage of elements identifiable on the records

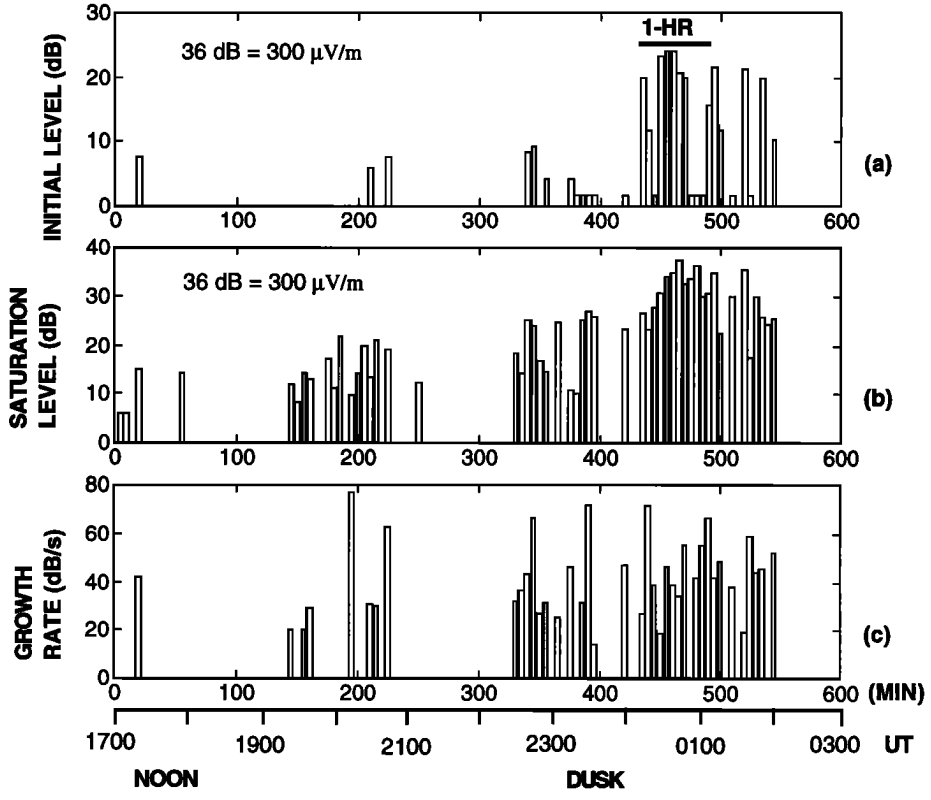

Figure 9. (a) Initial level, (b) saturation power level, and (c) growth rate of signal 5 over the 9-hour time period.

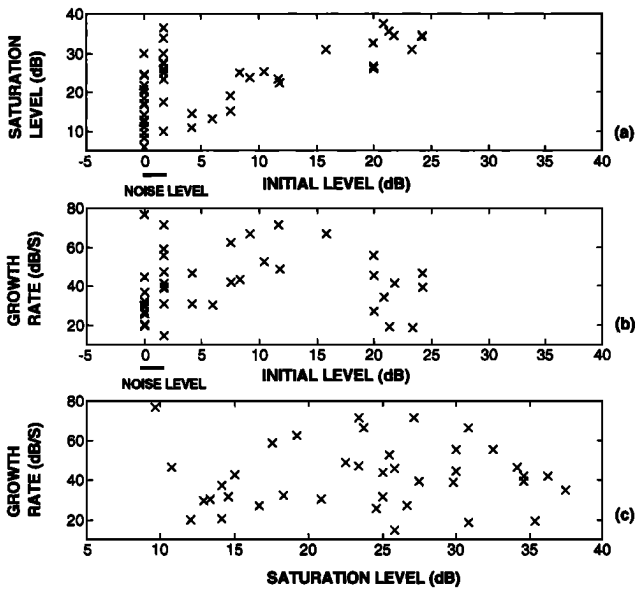

Figure 10. Scatterplots of the relationships between pairs of the signal 5 quantities shown in Figure 9 over the 9-hour study period. (a) Saturation power level versus initial power level. (b) Growth rate versus initial power level. (c) Growth rate versus saturation power level.

(Figure 6) and saturation power level (there are fewer data points in Figure 9 than in Figure 6 because of problems in measuring weak signals). On average, the growth rate and saturation level increased with time, leading to the interval from ~0015 to ~0110 UT when the percentages of format element occurrence shown in Figure 6 reached a peak. In particular, the saturation level increased from an average near 10 dB to about 30-35 dB from 1700 to 0200 UT. The initial level was measurable only rarely early in the period but after ~2200 UT was discernible more frequently and then jumped to high levels during the ~0015-0110 UT period of highest saturation levels and growth rates.

Figure 10 contains scatterplots relating saturation level and initial level, growth rate and initial level, and growth rate and saturation level. There is no discernible correlation between growth rate and either initial level or saturation level. In Figure 10a there appears to be a positive correlation between saturation level and initial level in those cases in which the initial level was above the noise level on the amplitude record (indicated at left by a dark horizontal bar). However, this correlative effect is believed to be due to the effects of changes in ionospheric absorption from noon to post-dusk on both the initial and saturation levels (see later comments on absorption), and not to a wave-hot plasma interaction mechanism. This is clearly indicated in the top two panels of Figure 9. Between ~0000 and 0200 UT the initial level underwent wide excursions at times when the saturation level was relatively high and steady. Furthermore, as shown in Figure 10a, when the initial level was at or below the noise level, the saturation level still varied over a wide range. Measurements such as those reported in Figures 9 and 10 were also made on element 7, with similar results.

3.4.2. Single duct period. The 60-min period 0015-0110 UT (bar above top panel in Figure 9) was selected to investigate in detail the effects of wave-particle interactions and in particular to study time variations both within ~1-min recording intervals and on the ~5-min timescale separating those intervals. As shown in Figure 7, propagation during this period took place essentially along a single duct, thus simplifying analysis of the data.

In order to separate hot plasma effects from propagation conditions, we compared the response at Lake Mistissini to the variously polarized signals 1 (RH), 2 (LH), and 3 (L, linear) of the format (Figure 3). Even if the duct were in the magnetic meridian of Siple, the field lines of the active duct at L = 5.1 would be at least 290 km from Siple station, so that the angle of incidence of the wave at the ionosphere would be oblique and the transmitted polarizations would be modified during coupling to the ionosphere [*Mielke et al.*, 1992]. However, the left-hand signal would be expected to couple least effectively (only a small fraction of LH polarized signal 2 would couple into the ionosphere as propagating RH polarization), and this was borne out by a comparison of peak amplitudes, as shown in Figure 11. In contrast to the levels of the right-hand and linear signals, the nearly constant peak level of the left-hand-transmitted signal throughout the period (middle panel), implies that it was below the threshold for temporal wave growth and thus did not undergo temporal amplification. Most importantly, this result implies that propagation factors along the ground-to-duct-to-ground circuit did not change during the 0015 UT to 0110 UT period.

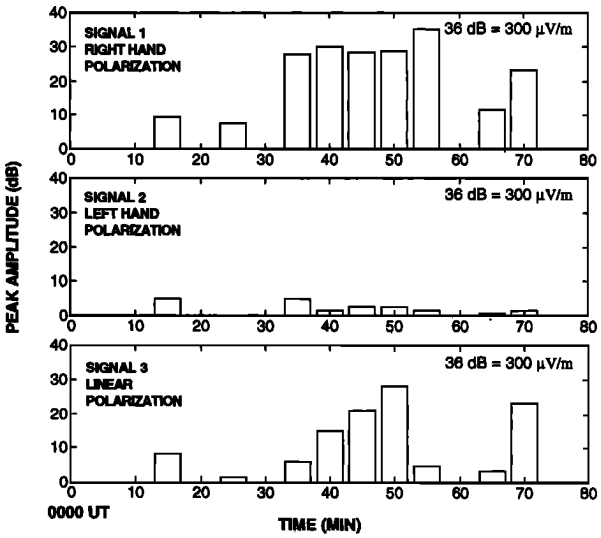

Figure 11. Peak power levels for signals 1 (right hand (RH)), 2 (left hand (LH)), and 3 (Linear (L)) during the time period 0015 - 0110 UT on January 24, 1988. For signals 1 and 3, peak levels represent saturation levels. The amplitude profile and peak values of signal 2 indicated that it had not undergone temporal wave growth.

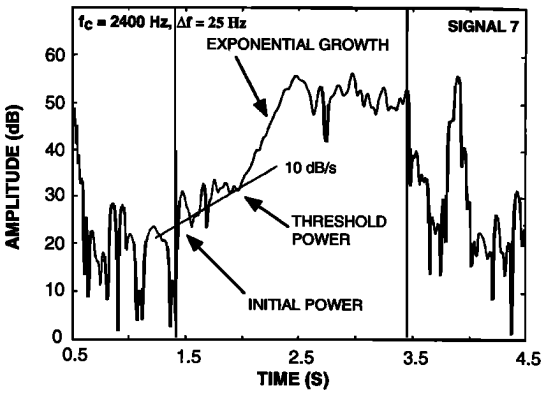

Figure 12. Example of the amplitude (f_c = 2400 Hz, Δf = 25 Hz) of signal 7, the amplitude ramp, during the transmission at 0115:40 UT on January 24, 1988. The first half second shows a power increase at 10 dB/s attributable to the 10 dB/s increase in transmitted power. After the first half second, a much steeper slope is seen which can be attributed to exponential growth due to wave-particle interactions. The power level at which this change occurs is identified as the threshold level for the onset of temporal wave growth.

Further evidence that element 2 (LH) was not amplified comes from comparing its peak level with the threshold level for wave-particle interactions measured within the same minute. Figure 12 shows how threshold power during transmissions at 0115 UT could be determined from the right-hand-polarized element 7, which began with a 1-s power ramp. The first half second, beginning at the left-hand vertical line, shows a power increase at 10 dB/s, attributable to the initial 10 dB/s increase in transmitted power. After the first half second a much larger growth rate was seen, which can be attributed to exponential growth due to wave-particle interactions. The power level at which this second exponential growth began is identified as the threshold level for the onset of temporal wave growth [*Helliwell et al.*, 1980; *Mielke and Helliwell*, 1992]. In four of the twelve cases (within the hour), the threshold level measurement could be performed. Figure 13 compares the initial and threshold levels of element 7 (RH), the initial level of element 5 (RH), and the peak level of element 2 (LH) for those four cases. In each the peak level of element 2 was below the threshold level of element 7, confirming that element 2 (LH) did not undergo temporal growth. Thus we can attribute observed temporal variations in the signal properties such as initial level, saturation level, growth rate, sideband bandwidth, and threshold level to corresponding variations in wave-particle interactions, that is, to hot plasma effects.

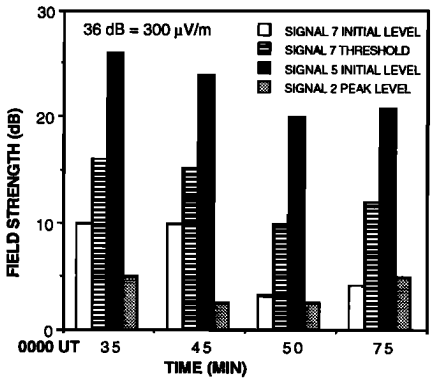

Figure 13. Comparisons of the initial and threshold levels of signal 7 (RH), the peak level of signal 2 (LH), and the initial level of signal 5 (RH). In each case the peak level of signal 2 was below the threshold level, confirming that signal 2 did not undergo significant temporal wave growth.

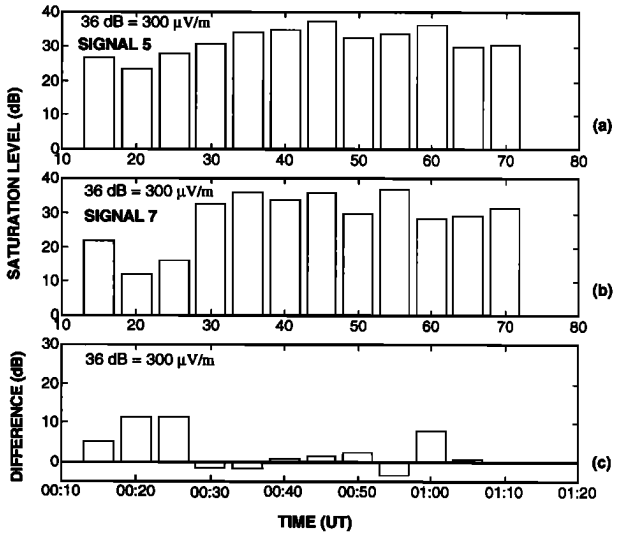

Figure 14. Saturation levels of (a) signal 5 and (b) signal 7 over the time period 0015 - 0110 UT. (c) The difference between signal 5 and 7 saturation levels.

Figures 14 through 16 provide comparisons of measurements on elements 5 and 7 during the 0015-0110

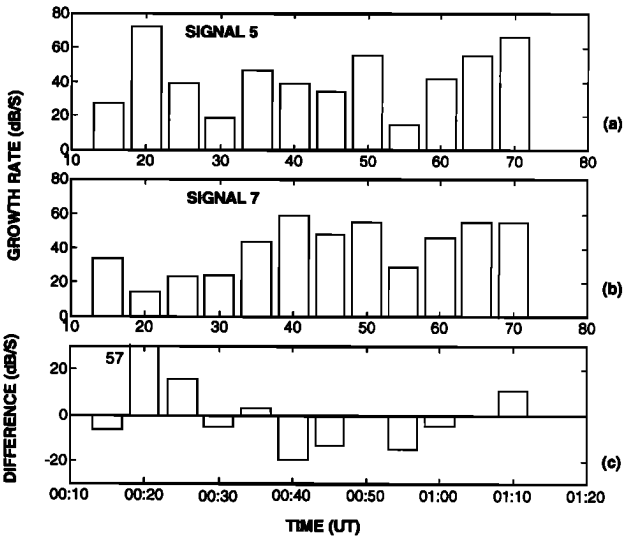

Figure 15. Growth rates of (a) signal 5 and (b) signal 7 over the time period 0015 - 0110 UT. (c) The difference between signal 5 and 7 growth rates.

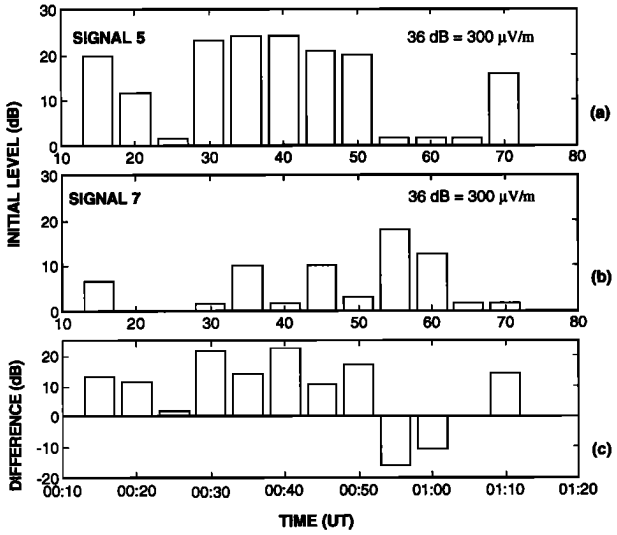

Figure 16. Initial power levels of (a) signal 5 and (b) signal 7 over the time period 0015 - 0110 UT. (c) The difference between signal 5 and 7 initial power levels.

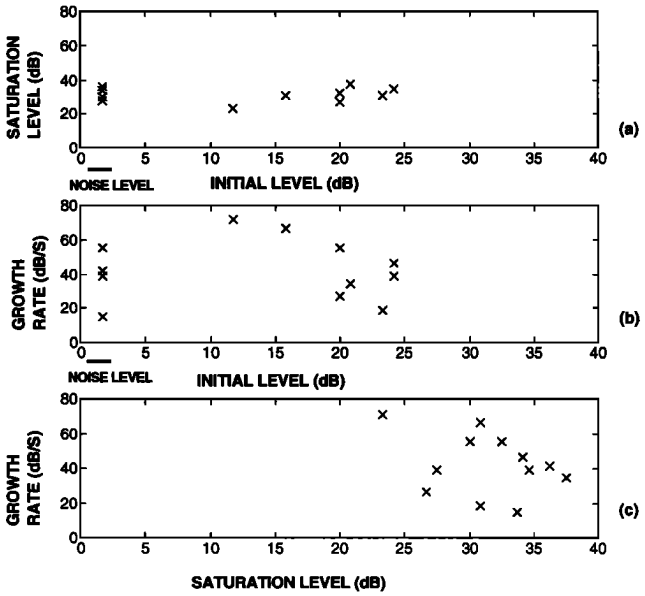

Figure 17. Scatterplots of the relationships between pairs of the quantities shown in Figures 14-16 for signal 5 over the time period 0015 - 0110 UT. (a) Saturation power level versus initial power level. (b) Growth rate versus initial power level. (c) Growth rate versus saturation power level.

UT period (both were 2-s constant frequency pulses, but element 7 was ramped linearly up to full power at 10 dB/s during the first second). Figure 14 shows the measured saturation levels and their differences. Element 5 exhibited an initial increasing trend and then relatively steady levels, such that during the hour most values were within ± 5 dB of 30 dB. Element 7, following element 5 by ~20 s, at first exhibited values lower than those of element 5 by ~10 dB, but beginning at 0030 reached levels very close to those of element 5.

Figure 15 shows the measured growth rates for elements 5 and 7 and their differences. With the exception of the 0020 UT case, there appear to have been comparable growth rates on the two elements. Larger run-to-run changes are indicated than were seen in the saturation level (Figure 14), but some of this variation may be attributed to the greater uncertainty in making the growth rate measurements.

The initial levels of elements 5 and 7 and their differences are plotted in Figure 16. On element 5 there were large run-to-run variations both early and late in the ~60-min period of interest. The leading edge of element 7, having been transmitted at -10 dB with respect to the leading edge of element 5, might have been expected to exhibit a level ~10 dB below that of element 5, provided all wave growth along the path was temporal in nature. When measureable it was in fact below the element 5 values in all cases except 3 near 0100 UT. However, the difference was variable between 22 and -16 dB.

Reviewing the temporal variations indicated, it appears that in general the saturation level could change significantly on timescales of 5-15 min. It remained nearly constant over the intervals of ~24 s separating elements 5 and 7 during most of the 1-hour period examined, although it appeared to decrease by ~10 dB within 24 s during three runs at the beginning of the 1-hour period. Comparisons of elements 5 and 7 in earlier parts of the 9-hour period showed generally similar relationships. Growth rates were found to change significantly on timescales of 5-15 min (Figure 15), but with the exception of one run did not vary more than ~ 20 dB/s on a timescale of ~24 s.

In Figure 17, plots of saturation level and growth rate versus initial level and of growth rate versus saturation level reveal no clear correlations within the ~60-min period, in agreement with the data of Figure 10 for the 9-hour period.

Figure 18 shows the received signal bandwidth at the saturation level of element 5 during the 1-hour period. This spectral broadening effect, which may be seen qualitatively in the spectrogram of Figure 5a and in the sideband fluctuations shown in Figure 5b, remained nearly constant at 20 Hz over the entire interval. This is consistent with previous observations in which the sideband frequency bore no simple relationship to the carrier amplitude, in our case the saturation levels [*Park*, 1981].

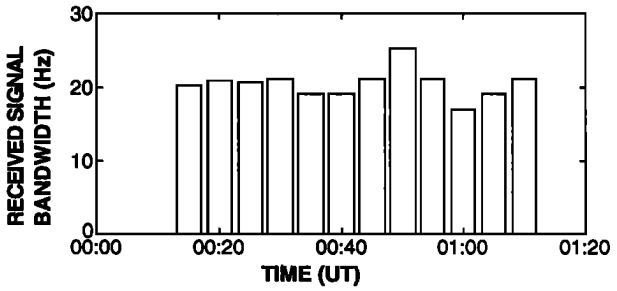

Figure 18. Bandwidth of the signal received (signal 5) at Lake Mistissini during the period 0015-0110 UT.

4. Interpretation

Schematics shown in Figures 1a and 1b illustrate various factors that are believed to influence the Siple signal levels detected at Lake Mistissini. These factors, listed below, can be classified broadly as those affecting passive propagation aspects of the waves and those related to the wave amplitude spectra through the phase space characteristics and the bounce and drift motions of the energetic particles.

1. Coupling of transmitter signals into the duct: these factors include transmission coefficients at the earth-ionosphere boundary, D and E region absorption losses, and coupling of upgoing waves into the duct. Taken together, these effects are indicated as ionospheric losses in Figure 1a. The transmission losses are strong functions of wave frequency, injection latitude and the local time [e.g., *Helliwell*, 1965; *Scarabucci*, 1970]. In our experiment, the wave frequency and injection latitude remained constant, but local time varied from noon to dusk (see Figure 6).

2. Passive propagation of signals from the southern hemisphere ionosphere to the equator: the signals undergo spreading losses in the duct.

3. Gyroresonant wave-particle interactions in an interaction region (about 2000 km in length) near the equator: the strength of the interaction depends both on the flux levels and the details of the particle distribution function near the equator [e.g., *Helliwell*, 1967; *Carlson et al.*, 1990].

4. Longitudinal, or Landau, resonance wave-particle interactions along the magnetospheric field line path: this mechanism gives rise to spatial growth or damping, in contrast to the temporal effects involved in (3).

5. Passive propagation of signals from the equatorial region to the conjugate ionosphere: the signals undergo focusing as they propagate downward. Generally, this focusing gain will cancel the spreading losses sustained by the upgoing signals.

6. Coupling of the signals from the duct exit point to the receiver: the signals undergo losses due to reflection, absorption, and spreading between the duct exit point at an altitude of 1000-2000 km and the lower ionospheric boundary [*Bernhardt and Park*, 1977; *Tsuruda et al.*, 1982]. The signals also experience spreading losses in the earth-ionosphere cavity.

The total signal at the receiver is the sum of the signals from all ducts and any ambient noise.

4.1. Cold Plasma Propagation

An important simplification of VLF hot plasma diagnostics occurs because the real part of the refractive index for whistler mode propagation is almost independent of the presence of hot plasma [*Kennel and Petchek*, 1966]. Thus propagation characteristics such as time delay as a function of frequency (dispersion) can be used to determine duct locations and cold plasma densities [e.g., *Carpenter and Smith*, 1964].

As discussed earlier, a duct (duct 1) at L=5.1 (invariant latitude = 64°) with equatorial cold plasma density $N_e \sim 276$ electrons/cm^3 appeared to be present for the entire 9-hour period. A second duct (duct 2) with time delay at 2400 Hz of 4.4 s was active during eight 1-min intervals, in five of which duct 1 was also present. Assuming that the electron density in the second duct was about the same as in the first, we estimate that this duct was located near $L \sim 5.6$. The fact that the second duct was significantly less active than the first can be attributed to its greater distance from the transmitter and receiver and perhaps also to insufficient fluxes of energetic electrons.

In the following, we discuss the signals propagating through duct 1.

4.2. Hot Plasma Effects: Estimate of Energetic Particle Parameters in Duct 1

We assume the following:

1. The interactions involving exponential growth and saturation took place near the equator over a distance equal to $L_{\text{int}} \sim 2000$ km.

2. The temporal changes in signal parameters such as growth rate and saturation level, indicative of wave-particle interactions inside the interaction region, were related to the energetic electron properties. These can be described by a distribution function $f(\mathbf{x}, V, \alpha, t)$, assuming that the distribution function was uniform over the azimuthal angle in velocity space.

3. The interactions within the interaction region were governed by first-order gyroresonance, which requires

$$\omega + k_{\|} V_{\|,eq} = \omega_H, \tag{1}$$

where ω, $k_{\|}$, $V_{\|,eq}$, and ω_H are wave angular frequency, parallel component of the wave normal vector, electron parallel velocity at the equator, and electron gyrofrequency, respectively. Now we can proceed to calculate various parameters of the hot plasma inside the duct.

Since ω, ω_H, and the electron plasma frequency ω_{pe} (from L=5.1 and $N_e = 276$ electrons/cm^{-3}) are known, we can determine $k_{\|}$ for ducted whistler mode propagation from the following relations.

$$k = k_{\|} = \omega\mu/c, \quad \mu^2 = 1 + \frac{\omega_{pe}^2/\omega^2}{(\omega_H/\omega) - 1}, \tag{2}$$

where μ is the whistler mode refractive index. Then, as shown in Figure 19a, we can use (1) to calculate $V_{\|,eq}$ as a function of frequency. The presence in our case of electrons with $V_{\|,eq} \sim 1.0 - 1.5 \times 10^7$ m/s is indicated by the amplification of signals at frequencies between 1.9 and 2.55 kHz. Since ionospheric losses are expected to vary smoothly with frequency, the absence of signals between 2.55 and 2.90 kHz, a range below the previously mentioned propagation cutoff at 3.3 kHz, can be attributed to a lack of electrons with appropriate $V_{\|,eq}$. Figure 19b shows regions (indicated by arrows) in particle phase space where particles were inferred to be "present" and "absent," as well as the loss cone. This interpretation is consistent with recent observations of banded structures ("clouds") of electrons within the plasmasphere ($2 < L < 6$) [*Burke et al.*, 1995].

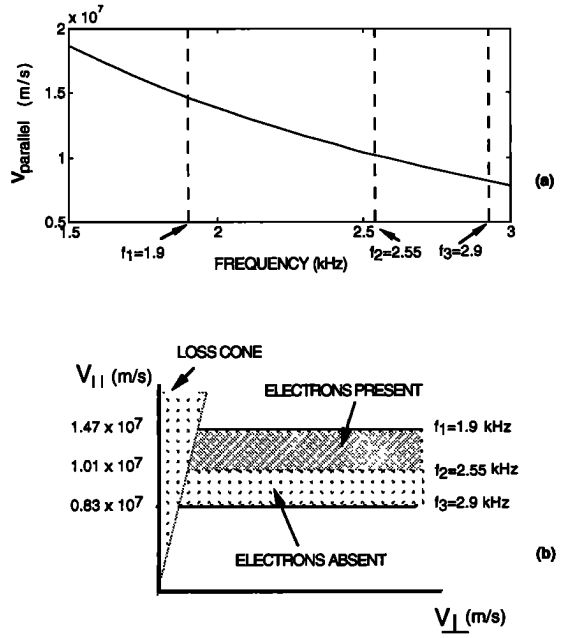

Figure 19. (a) $V_{\|}$ of particles in gyroresonance with whistler mode waves along the observed $L = 5.1$ propagation path. The dashed vertical lines indicate the limiting frequencies of transmitted signals for which wave growth was observed (between f_1 and f_2) or was not observed (between f_2 and f_3). (b) Schematic showing the inferred "presence" and "absence" of particles in velocity space, based on the wave growth observations.

Under adiabatic theory in a static magnetosphere, the dynamics of electrons with a given $V_{\|}$ in the geomagnetic field are completely determined as a function of the equatorial pitch angle α_{eq}. Thus, for a given $V_{\|,eq}$ we can calculate the kinetic energy E, bounce period τ_b and longitudinal drift period τ_d of electrons as a function of the equatorial pitch angle α_{eq}. These quantities, with approximate expressions for τ_b and τ_d, are given below [*Walt*, 1994].

$$\tan \alpha_{eq} = \frac{V_{\perp,eq}}{V_{\|,eq}} \tag{3}$$

$$\beta = \frac{V}{c} = \frac{[V^2_{\perp,eq} + V^2_{\|,eq}]^{1/2}}{c}; \quad \gamma = (1-\beta^2)^{-1/2} \tag{4}$$

$$E = (\gamma - 1) m_0 c^2 \tag{5}$$

$$\tau_b(s) = 0.117 \frac{L}{\beta}[1 - 0.4635(\sin \alpha_{eq})^{3/4}] \tag{6}$$

$$\tau_d(s) = 1.557 \times 10^4 \frac{1}{L\gamma\beta^2}[1 - 0.333(\sin \alpha_{eq})^{0.62}] \tag{7}$$

Figures 20a to 20c show electron energy, bounce period, and drift period as a function of pitch angle for a parallel velocity of 1.1×10^7 m/s, corresponding to an electron in gyroresonance with 2.4-kHz signals.

It is important to consider how much time an electron will spend inside a duct as a result of longitudinal drift. Assuming the duct width in longitude to be $\sim 4°$ [*Angerami*, 1970], we can estimate this "duct period" as shown in Figure 20c. The whistler mode wave refractive index at 2.4 kHz was 47.2 at the equator inside the $L = 5.1$ duct and the corresponding wavelength was 2.64 km. Thus the duct was about 136 wavelengths wide in the east-west direction. The evidently highly coherent nature of wave-particle interactions involving Siple transmitter signals [*Helliwell et al.*, 1986a] suggests that the width of the interaction region cannot be greater than a few wavelengths (this assumption is based on the fact that the gyroradius of 1 keV electrons in the duct was about 0.45 km and at 10 keV was about 1.4 km; entirely different sets of electrons presumably interacted with waves separated in longitude by a few kilometers or a few whistler mode wavelengths). Thus more than one interaction region may exist within a single duct, and depending on the fine structure of the duct (which will determine the fine structure of the waves present inside the duct), one or more interaction regions may be active at a given time. Assuming the longitudinal width of an interaction region to be five whistler mode wavelengths at 2.4 kHz, we can calculate $T_{\text{int,long}}$, the time that an electron spends within the region, as a function of pitch angle. This time period is shown in Figure 20d.

There is one more timescale of interest, the time during which an electron undergoes gyroresonant interactions with the wave. *Helliwell* [1967, 1970] has estimated the interaction length to be of the order of 1000-2000 km for second-order resonance. The interaction region is located where the curve of Doppler-shifted wave frequency as a function of distance along the field line is tangent to the corresponding curve of electron gyrofrequency. The point where the resonance interaction occurs is a function of df/dt [e.g., *Carlson et al.*, 1985].

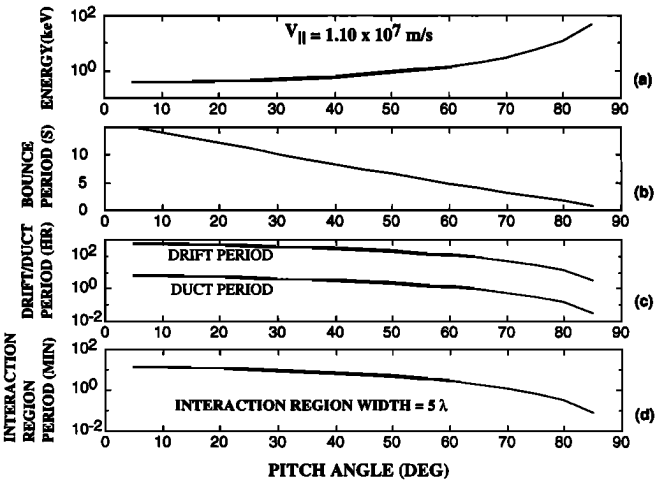

Figure 20. (a) Resonant particle energy, (b) bounce period, (c) drift and duct periods, and (d) interaction region period as a function of pitch angle, based on the parameters of duct 1, $V_{\|} = 1.10 \times 10^7$ m/s, and assumptions detailed in the text.

For constant frequency pulses ($df/dt = 0$), the resonant interaction is "centered" on the magnetic equator, and the interaction length corresponds to an interaction time of 100-200 ms for an electron with a parallel velocity of 1.1×10^7 m/s.

Since the Kp index during the 12-18 hour interval

special 1-hour study we found that with a brief exception near the beginning of the activity surge: (1) the saturation levels did not change over a timescale of 30 s (Figure 14c), consistent with previous data on variable-pulse-length transmissions [*Helliwell and Katsufrakis*, [1974]; (2) the growth rate changed only slightly, by less

4.2.3. Bounce motion of the electrons. The bounce periods of the energetic electrons of interest with pitch angles of 40° to 80° are between 8 and 2 s. Thus, for a given 2 s-long pulse (elements 5 and 7), most of the electrons present in the duct should have participated in the wave-particle interaction. Depending on their pitch angles, the particles that interacted with element 5 would undergo 3 to 12 bounce period motions before interacting with element 7. Because the bounce period of a particle is a function of pitch angle, the pitch angle distribution of the particles interacting with element 7 would, in general, be different from that of the particles that interacted with element 5. The observations showed mostly similar saturation levels for elements 5 and 7; growth rates for the 2 elements were on average about the same, but did exhibit differences of the order of ±10 dB/s within a single 1-min run. Thus we infer that while element 5 did not strongly perturb the initial particle distribution, in conjunction with the immediately preceding element 4 it may have modified the distribution function sufficiently to cause a modest increase or decrease in the growth rate.

4.2.4. Relation of wave parameters to particle parameters. Our next task is to relate the signal properties such as growth rate and saturation level to particle properties such as flux and pitch angle anisotropy so that we can study the particle properties within the duct as a function of time. To make this connection, it is necessary to have a detailed model of the wave-particle interaction that connects the particle and wave parameters. Two different models have been proposed to account for the observed temporal wave amplification and saturation: a small signal model and a large signal model (see *Helliwell* [1988] and *Carlson* [1987] for a discussion of these models). In the following, we adopt the *Carlson et al.* [1990] small signal model which, we believe, explains many features of our data. In addition to predicting exponential growth and saturation (of the same order of magnitude as observed), this model predicts that wave growth rate and saturation levels are independent of initial signal levels, consistent with our observations (Figures 10 and 17). Two results from this model can be used to interpret saturation levels and growth rates in terms of particle parameters:

1. The final saturation level is dependent only on the total flux of energetic particles in resonance with the waves and is independent of the initial signal level and the details of the pitch angle distribution, at least for the specific cases considered by *Carlson et al.* [1990].

2. The growth rate depends on the total flux of energetic particles in resonance with the waves and also on the details of the pitch angle distribution but is independent of the initial signal level.

Our observations show that saturation levels and growth rates were not related. Combining this result with the two results from modeling, we can infer that (1) the observed variations in saturation level were a direct measure of the total flux of resonant electrons ($E = 0.6 - 11$ keV, $40° < \alpha < 80°$); and (2) the observed growth rates reflected the distribution of energetic electrons in pitch angle. If we make use of *Carlson et al.*. [1990] result that a pitch angle distribution peaked at 45° leads to the largest growth rates, then for constant saturation levels (and therefore constant flux levels), our growth rate results provide an indication of the relative fraction of particles near 45° pitch angle.

Study of more detailed relations linking signal saturation levels and growth rates to electron flux and anisotropy would require detailed computer modeling, which is beyond the scope of this paper.

5. Diagnostic Potential of Pulse Initial Levels

We need to investigate the diagnostic potential of the initial level, that is, the amplitude of the pulse leading edge. That amplitude may provide a measure of the input signal level on which a temporal growth process operates, but by definition is not itself a product of that process. Relevant points are as follows:

1. Leading edge amplitudes were readily measurable in the cases of most constant-frequency, constant-power pulses that could be identified on spectrograms.

2. In the case of elements 5 and 7 (Figure 16), the leading edge amplitude varied over a range of 20 dB within the hour of interest while the peak amplitude of the left-hand polarized element 2 (the same as its initial value), considered to be a measure of passive propagation conditions, varied by only 1-2 dB (Figure 11).

3. The leading edge amplitude of a 2-s pulse was uncorrelated with the growth rate and saturation level observed within the same pulse.

The exponential temporal growth process that takes place near the equator, and discussed extensively in the literature [see *Carlson et al.*, 1990 and references therein], does not predict amplification of the leading edge of a signal. Point 2 above clearly indicates that leading edges of elements 5 and 7 underwent amplification during the one hour period of interest; furthermore, as noted in point 3, this amplification was uncorrelated to growth rate and saturation level, parameters related to temporal exponetial growth process. Therefore these results suggest that the leading edge amplitudes were controlled by the hot plasma, but in a manner independent of the process giving rise to exponential temporal growth and saturation within the same pulses. We attribute the amplification of the leading edges to a new hot plasma process that involves spatial amplification of transmitter signals. Assuming that spatial amplification was involved, the left-hand polarized (element 2) pulses at the same frequency might have been expected to exhibit changes comparable to those of element 5. The fact that they did not (point 2) is not understood, but could be due to the low level of the injected element 2 and possible nonlinearity in the amplification process. Some type of threshold for spatial growth may have existed, analogous to that found in the case of temporal growth (and illustrated in Figure 12). Evidence for the

action of a second (spatial) hot plasma process is further discussed in paper 2.

6. Potential of a Ground-Based Wave Injection Facility for Hot Plasma Diagnostics

Ground-based cold plasma magnetospheric diagnostics using the whistler method have been in use for more than 3 decades. The special advantages of controlled wave injection in this area are the following: (1) The source time and location are accurately known; (2) the source amplitude spectrum is known; and (3) the source power and wave form can be adjusted to minimize wave growth and thus permit identification of changes in propagation conditions such as ionospheric absorption.

Our observations and analysis suggest that a ground-based wave injection facility could be used to perform diagnostics of both the cold and hot plasmas of the magnetosphere. We have shown that in a case study, signal properties ascribable to cold plasma propagation and to interactions of the waves with energetic electrons could be separately identified, allowing simultaneous diagnostics of hot and cold plasma along a whistler mode signal path in the outer plasmasphere.

7. Possibility of Hot Plasma Diagnostics Using Natural Wave Activity

During the 15 years of wave injection experiments, regular recordings of data on natural VLF emissions such as whistlers, hiss, and chorus were made in the 0.3-20 kHz frequency band. Natural emissions and whistlers play a significant role in magnetospheric energy and momentum exchange with particles, but because of their diversity and complexity they have not been studied systematically with respect to their dependence upon the hot plasma. The previous section suggests that comparing time series analyses of artificially injected signals and of natural VLF activity may be a good starting point, since our experience with Siple transmitter signals would serve as a guide and reference. Several previous studies indicate that similar mechanisms may be operating for the growth and triggering of natural and artificial signals. If we can establish that this is the case, we can then use natural VLF activity to investigate the hot plasma environment inside a duct as a function of time.

8. Summary and Concluding Remarks

We have provided new observations and analyses of Siple Station wave injection experiments. A case study of a 9-hour period on January 23-24, 1988, during most of which a single whistler path was active, has led to the following new findings about wave-particle interactions with Siple transmitter signals:

1. The initial levels, saturation levels, and growth rates of single-frequency constant power pulses were not correlated, except for the expected dependence of initial level and saturation level on the path attenuation.

2. With the exception of a ~10-min period near the beginning of a ~1-hour surge in signal activity, the saturation levels of two pulses injected within 30 s were the same within a few dB. Growth rates for the two pulses were typically in the 30-50 dB/s range and tended to agree within ±10 dB/s.

3. The initial level, saturation level, and growth rate showed temporal variations over 5–15 min and 1–2 hour timescales.

4. The leading edges of constant frequency signals underwent spatial amplification.

5. The received signal bandwidth remained constant over a 1-hour period, although the initial level, saturation level, and growth rates varied during the same period.

Measured time delays and dispersion of the signals were used to determine the duct L-shell and electron density within the duct, which in turn led to the determination of $V_{\parallel,eq}$ for energetic electrons interacting with the waves via gyroresonace. The frequency range of the waves exhibiting wave-particle interaction effects and the various timescales over which saturation and growth rates varied or remained constant led to the determination of energetic electron parameters in velocity space. We interpreted the temporal variations in the wave parameters (saturation level and growth rate) in terms of variations in particle parameters (flux and anisotropy) as the interacting particles drifted longitudinally in and out of the duct. Assuming the *Carlson et al.* [1990] wave-particle interaction model, the changes in saturation levels could be directly related to the changes in flux of the resonant energetic electrons. Further work on theories of wave-particle interactions is needed to establish one-to-one connections between the wave and particle parameters.

Specifically, our analysis indicates that in the interval 1700-0210 UT on January 23-24, 1988, electrons with energy between 0.6 and 11 keV and pitch angle between 40° and 80° were present at varying levels in a duct at $L = 5.1$ near the Siple station longitude. In the reference frame of the duct and during most of a period of enhanced wave-particle interaction activity, the particle fluxes showed no variation over a 30 s timescale but did vary significantly over 5-15 min and 1-2 hour timescales. The longitudinal drift period of 11 keV electrons at $L = 5.1$ with equatorial pitch angle of 80° is 12 hours, while the drift period of 0.6 keV electrons with 40° pitch angle is 275 hours. These drift rates define the longitudinal extent of the energetic electron structures responsible for 5–15 min fluctuations and the 1–2 hour time variations seen in the transmitter signals. For the short term fluctuations, longitudinal structures of the order of 0.2° in longitude or 100 km in the equatorial plane are required for 0.6 keV, 40° pitch angle electrons. The higher-energy electrons at 80° pitch angle would need a dimension of 5° in longitude or 2800 km. The hour-long variations imply hot plasma structures of 2° in longitude or 1100 km for the 0.6-keV electrons and 45° or 25,000 km for the 11-keV electrons.

It would be interesting to compare these results with in situ data from satellites. Such a comparison with existing data, however, is difficult because data at a point fixed with respect to the rotating earth can only be obtained at geosynchronous orbit ($L \sim 6.6$). Available in situ electron data in the energy range of interest (0.5-11 keV) are (1) from the OGO 3 satellite (perigee=$1.1R_E$, apogee=$20.1R_E$, inclination = 30°), which measured differential spectra of protons and electrons extending from 100 eV to 50 keV [e.g., *Schield and Frank*, 1968], (2) from AMPTE/CCE satellite (perigee is $0.17R_E$, apogee is $8.79R_E$, inclination is 4.8 °), which measured fluxes of electrons between 50 eV and 25 keV [e.g., *Shelly et al.*, 1985], and (3) from CRRES satellite (perigee is 350 km, apogee is $5.6R_E$, inclination is 18.2 °), which measured fluxes of electrons and ions between 10 eV and 30 keV [e.g., *Hardy et al.*, 1993]. It is difficult to compare these data sets with our results because these satellites cover large ranges of L values and longitudes over a few hour timescales. However, recently reported CRRES observations of banded structures (clouds) of electrons at ~500 eV and at 1-30 keV within the plasmasphere ($2 < L < 6$) [*Burke et al.*, 1995] are consistent with the azimuthal structure of hot electrons indicated by our study. The impossibility of obtaining satellite particle data at an arbitrary fixed point with respect to the earth and the difficulty in separating temporal and spatial changes in satellite particle data point to the desirability of developing a ground-based diagnostic facility for studying the radiation belt hot plasma.

Because of variations in drift rate with electron energy and equatorial pitch angle, azimuthal structures of the kind reported here will necessarily change with time and as a function of observing longitude. However, injected whistler mode waves often propagate simultaneously on multiple discrete paths [e.g., *Leavitt et al.*, 1978]. Thus additional information on the particle energy and pitch angle distribution might be obtained by sensing and processing techniques that isolate the signals received from paths separated in longitude. The potential of such techniques for signal isolation has been demonstrated by spaced receiver observations [*Tsuruda et al.*, 1982] and by direction finding from a single site [*Leavitt et al.*, 1978].

We found that the leading edge of constant-frequency pulses underwent amplification, indicating the presence of a spatial amplification process in the magnetosphere. Further evidence for such a process is provided in a companion paper [*Carpenter et al.*, this issue] which discusses the temporal variations of wave-particle interactions at multiple frequencies.

Acknowledgments. The research at Stanford was sponsored by the Division of Polar Programs of the National Science Foundation under grant DPP89-18326 and previous grants for work at Siple Station.

The Editor thanks O. W. Lennartsson and W. F. Denig for their assistance in evaluating this paper.

References

Angerami, J. J., Whistler duct properties deduced from VLF observations made with the OGO-3 satellite near the magnetic equator, *J. Geophys. Res., 75,* 6115, 1970.

Bernhardt, P. A., and C. G. Park, Protonospheric-ionospheric modeling of VLF ducts, *J. Geophys. Res., 82,* 5222, 1977.

Burke, W. J., A. G. Rubin, D. A. Hardy, and E. G. Holeman, Banded electron structures in the plasmasphere, *J. Geophys. Res., 100,* 7759, 1995.

Carlson, C. R., Simulation and modeling of whistler mode wave growth through cyclotron resonance with energetic electrons in the magnetosphere, Ph.D. thesis, Stanford Univ., Stanford, Calif., 1987.

Carlson, C. R., R. A. Helliwell, and D. L. Carpenter, Variable frequency VLF signals in the magnetosphere: Associated phenomena and plasma diagnostics, *J. Geophys. Res., 90,* 1507, 1985.

Carlson, C. R., R. A. Helliwell, and U. S. Inan, Space-time evolution of whistler mode wave growth in the magnetosphere, *J. Geophys. Res., 95,* 15,073, 1990.

Carpenter, D. L., Ducted whistler-mode propagation in the magnetosphere; a half gyrofrequency upper intensity cutoff and some associated wave growth phenomena, *J. Geophys. Res., 73,* 2919, 1968.

Carpenter, D. L., and R. R. Anderson, An ISEE/whistler model of equatorial electron density in the magnetosphere, *J. Geophys. Res., 97,* 1097-1108, 1992.

Carpenter, D. L., and R. L. Smith, Whistler measurements of electron density in the magnetosphere, *Rev. Geophys., 2,* 415, 1964.

Carpenter, D. L., V. S. Sonwalkar, M. Ikeda, R. A. Helliwell, U. S. Inan, M. Walt, and D. L. Caudle, Probing properties of the magnetospheric hot plasma distribution by whistler mode wave injection at multiple frequencies: Evidence of spatial as well as temporal wave growth, *J. Geophys. Res.,* this issue.

Edgar, B. C., The upper and lower frequency cutoffs of magnetospherically reflected whistlers, *J. Geophys. Res., 81,* 205, 1976.

Hamar, D., G. Tarcsai, J. Lientenberger, A. J. Smith, and K. H. Yearby, Fine structure of whistlers recorded digitally at Halley, Antarctica, *J. Atmos. Terr. Phys., 52,* 801, 1990.

Hamar, D., C. Ferencz, J. Lichtenberger, G. Tarcsai, A. J. Smith, and K. H. Yearby, Trace splitting of whistlers: A signature of fine structure or mode splitting in magnetospheric ducts? *Radio Sci., 27,* 341, 1992.

Hardy, D. A., D. W. Walton, A. D. Johnstone, M. P. Gough, A. Huber, J. Pantazis, and R. Burkhardt, The low energy plasma analyzer, *IEEE Trans. Nucl. Sci., 40,* 246, 1993.

Helliwell, R. A., *Whistlers and Related Ionospheric Phenomena,* Stanford Univ. Press, Stanford, Calif., 1965.

Helliwell, R. A., A theory of discrete VLF emissions from the magnetosphere, *J. Geophys. Res., 72,* 4773, 1967.

Helliwell, R. A., VLF wave stimulation experiments in the magnetosphere from Simple Station, Antarctica, *Rev. Geophys., 26,* 551, 1988.

Helliwell, R. A., and J. P. Katsufrakis, VLF wave injection into the magnetosphere from Siple Station, Antarctica, *J. Geophys. Res., 79,* 2511, 1974.

Helliwell, R. A., D. L. Carpenter, and T. R. Miller, Power threshold for growth of coherent VLF signals in the magnetosphere, *J. Geophys. Res., 85,* 3360, 1980.

Helliwell, R. A., U. S. Inan, J. P. Katsufrakis, and D. L. Carpenter, Beat excitation of whistler mode sidebands using the Siple VLF transmitter, *J. Geophys. Res., 91,* 143, 1986a.

Helliwell, R. A., D. L. Carpenter, U. S. Inan, and J. P. Katsufrakis, Generation of bank-limited VLF noise using

the Siple transmitter: A model for magnetospheric hiss, *J. Geophys. Res., 91*, 4381, 1986b.

Helliwell, R.A., Intensity of discrete VLF emissions, in *Particles and Fields in the Magnetosphere*, edited by B.M. McCormac, p. 292, D. Reidel, Norwell, Mass., 1970.

Jursa, A. S. (Ed.), *Handbook of Geophysics and the Space Environment*, Air Force Geophys. Lab., Hanscom Air Force Base, Mass., 1985.

Kennel, C. F., and Petschek, H. E., Limit on the stably trapped particle fluxes, *J. Geophys. Res., 71*, 1, 1966.

Kimura, I., Effects of ions on whistler-mode raytracing, *Radio Sci., 1*, 269, 1966.

Leavitt, M. K., D. L. Carpenter, N. T. Seely, R. R. Padden, and J. H. Doolittle, Initial results from a tracking receiver direction finder for whistler mode signals, *J. Geophys. Res., 83*, 1601, 1978.

Mielke, T. A., and R. A. Helliwell, An experiment on the threshold effect in the coherent wave instability, *Geophys. Res. Lett., 19*, (20), 2075, 1992.

Mielke, T. A., C. J. Elkins, R. A. Helliwell, and U. S. Inan, Excitation of whistler mode signals via injection of polarized VLF waves with the Siple transmitter, *Radio Sci., 27*, 31, 1992.

Park, C. G., Generation of whistler-mode sidebands in the magnetosphere, *J. Geophys. Res., 86*, 2286, 1981.

Paschal, E. W., and R. A. Helliwell, Phase measurements of whistler mode signals from the Siple VLF transmitter, *J. Geophys. Res., 89*, 1667, 1984.

Scarabucci, R. R., Satellite observations of equatorial phenomena and defocusing of VLF electromagnetic waves, *J. Geophys. Res., 75*, 69, 1970.

Schield, M. A., and L. A. Frank, Electron observations between the inner edge of the plasma sheet and the plasmasphere, *J. Geophys. Res., 73*, 1, 1968.

Shelley, E. G., A. Ghielmetti, E. Hertzberg, S. J. Battel, K. Altwegg-von Burg, and H. Balsiger, The AMPTE/CCE hot-plasma composition experiment (HPCE), *IEEE Trans. Geosci. Remote Sens., GE-23*, 241, 1985.

Smith, R. L., and J. J. Angerami, Magnetospheric properties deduced from OGO 1 observations of ducted and nonducted whistlers, *J. Geophys. Res., 73*, 1, 1968.

Sonwalkar, V. S., Magnetospheric LF-, VLF-, and ELF-waves, chap. II/13, *Handbook of Atmospheric Electrodynamics*, CRC Press, Boca Raton, Fla., April 1995.

Sonwalkar, V. S., T. F. Bell, R. A. Helliwell, and U. S. Inan, Direct multiple path propagation: A fundamental property of nonducted VLF waves in the magnetosphere, *J. Geophys. Res., 89*, 2823, 1984.

Sonwalkar, V. S., U. S. Inan, T. F. Bell, R. A. Helliwell, V. M. Chmyrev, Y. P. Sobolev, O. Y. Ovcharenko, and V. Selegej, Simultaneous observations of VLF ground transmitter signals on the DE 1 and COSMOS 1809 satellites: Detection of a magnetospheric caustic and a duct, *J. Geophys. Res., 99*, 17,511, 1994.

Tsuruda, K., S. Machida, T. Terasawa, A. Nishida, and K. Maezawa, High spatial attenuation of the Siple transmitter signal and natural VLF chorus observed at ground-based chain stations near Roberval, Quebec, *J. Geophys. Res., 87*, 742, 1982.

Walt, M., *Introduction to Geomagnetically Trapped Radiation*, Cambridge Univ. Press, New York, 1994.

D. L. Carpenter, R. A. Helliwell, U. S. Inan, and M. Walt, STAR Laboratory, Stanford University, Stanford, CA 94305. (e-mail: tsstar::carpenter; helliwell@sierra.stanford.edu; inan@sierra.stanford.edu; walt@nova.stanford.edu)

D. L. Caudle, Naval Postgraduate School, Monterey, CA 93943.

M. Ikeda, Musashi University, Tokyo 176, Japan. (e-mail: ikeda@musashi.ac.jp)

V. S. Sonwalkar, Institute of Northern Engineering, University of Alaska Fairbanks, Fairbanks, AK 99775. (e-mail: ffvss@aurora.alaska.edu)

(Received April 23, 1996; revised October 2, 1996; accepted October 2, 1996.)